Improving SERS substrates with Au/Ag-coated Si nanostructures generated by laser ablation synthesis in PVA

Qudama Kh. Hammad[1] · Adil N. Ayyash[1] ·
Falah A.-H Mutlak[2]

Abstract This paper provides an efficient approach for making effectual and active substrates utilized for the detection of the Pyrromethene 580 (PM 580) molecule through the improvement of surface-enhanced Raman scattering (SERS). Those substrates have been fabricated with the use of the Au/Ag nanoparticles-coated porous silicon (PS). Au/Ag NPs have been prepared through laser ablation technique. This investigation is comparing Au/Ag NPs characteristics that have been generated by nanosecond laser ablation in PolyVinyl Alcohol (PVA) at 532 nm and 1064 nm laser wave-lengths. Then, Au/AgNPs were ablated in PVA colloidal solution to form (AuNPs:AgNPs)/PS plasmonic nanostructures. These plasmonic nanostructures on the SERS activities were studied utilizing PM 580 dye as examination molecule. Results have shown that the roughness and spots on nanostructures surfaces have resulted in causing increased absorbance spectra intensities and SERS signals. After effectual substrates have been excited by (λex. $= 532$ nm) laser source, the enhancement factor (EF) of SERS signals of PM 580 (0.01 M) attained 13.7×10^7 and 5.6×10^7 of the characteristic peaks at wavenumber 1657 cm^{-1} for the Au:AgNPs-532 nm/PS and Au:AgNPs-1064 nm/PS effectual substrates, respectively. The present research had shown that the nanostructure-coated PS substrates have repeatable and high signal frequency, inexpensive technique, stability in storage, and simplicity of use.

Introduction

Since the advent of treatment activities of nanomaterials against bacteria and viruses, nano-sized materials have attracted much attention, partially as a result of their unique properties that set them apart from bulk materials [1–11]. One of the key nanomaterials is metal colloids, which are small particles of metal. Optical properties and strong catalytic activity have attracted the attention of scientists. Laser ablation in solutions has recently been shown to be a new potential approach for obtaining metal colloids [12–18]. Laser ablation removes the requirement for chemical reagents as compared to other ways of creating metal colloids [19–24]. It is feasible to create pure colloids in this manner, which may then be employed in various applications. Controlling particle size is critical when manufacturing colloid systems since the character of the nano-sized metal particles is strongly reliant on their size. Jeon et al. examined the connection between particle size and number of the laser pulses irradiating the particle [25]. The surface plasmon resonance (SPR) that is a resonant connection between electro-magnetic field frequency and free electrons oscillation frequency for the metal nano-particles, Metallic NPs cause a significant absorption of electromagnetic field energy when resonance conditions are matched [26]. Giorgetti et al. [27] used a picosecond laser to ablate metallic (Ag and Au) and semi-conductor (CdSe) target materials in the water at basic (1064 nm–25 ps), 2nd-harmonic (532 nm–20 ps), and 3rd-harmonic (355 nm–15 ps) laser wave-lengths for the production of the NPs. At 1064 nm, 532 nm, and 355 nm wavelength values, Au nanoparticles of different sizes were

✉ Qudama Kh. Hammad
Alsobahi733@gmail.com

1 Department of Physics, College of Science, University of Anbar, Anbar, Iraq

2 Department of Physics, College of Science, University of Baghdad, Baghdad, Iraq

produced: 5.2, 3.2, and 2.5 nm. A picosecond laser has been used to create silver nanoparticles in the liquid environment at the wave-lengths of 1064 nm [28]. The interaction of analyte molecules with the SERS substrate, which is usually a surface-roughened or nanostructured metal, is critical to the technique's operation [29]. In addition to greatly increasing Raman emission, SERS interactions may differ from those in a bulk Raman sample. SERS prove their flexibility through the following properties: they (a) combine the inherent properties of Raman identification abilities due to the vibrational fingerprints of the molecules; (b) involve a non-destructive analysis technique; (c) require a smallest amount of prepared sample; and (d) can carry out certain tests with their inherent advantages [30]. SERS substrates are often engineered to maximize hotspot density by using their enhancement performance to the fullest [31, 32]. Effectual substrates of SERS have largely been influenced by plasmonic noble metals (e.g., Au, Ag) and metal nanostructures with rough surfaces. Despite earlier research on effects of laser wave-length in nanoparticle laser production, the effects of laser wave-length in nanosecond laser production of the nano-particles are still unknown, as are the mechanisms involved. In this work, Au/Ag NPs were produced in PVA using nanosecond laser wave-lengths of 532 nm, and 1064 nm. The Au/Ag NPs have been compared then according to their morphology and sizes. Also, look at the SERS signal and detect molecules (PM 580 dye molecules) at exceptionally low concentrations.

Experimental details

Figure 1a illustrates laser ablation leads to production of Au/Ag NPs colloids in a laboratory. At the bottom of an ultra-pure PVA filled glass container, the gold and silver plate (> 99.99% purity) was deionized and re-distilled before being mounted. A quantity of polymer powder of 0.2 g was taken and dissolved using 20 ml of distilled water. After which it was placed on the magnetic stirrer for 30 min at a temperature of 50 °C to obtain a complete dissolution. Approximately 3 mm of PVA was applied to the gold foil. Ablation and dissolution of the colloid particles take place in a slow-moving solvent that is constantly agitated, prepared in an open air (aerobic) environment. The Q-Switched Nd:YAG laser system was used with energy of pulse 400–1000 mJ/pulse, a pulse length of 10 ns, and a 1 Hz repetition rate. A convex lens with a focal length of 12 cm was utilized for laser beams with diameters of 2.1 mm (for 532 nm), and 2.4 mm (for 1064 nm), respectively, and center section beam of the laser was chosen to monitor the intensity of unfocused point of laser light. Optical power detectors regulate and measure the light energy when laser lamp has discharge voltage. The Nd:YAG laser's primary (1064 nm), 2nd harmonic (532 nm) outputs were employed as irradiation sources.

After each ablation or fragmentation, 3 ml of the colloid solution. A quartz cell with a diameter of 1 cm was carried for UV–VIS optical spectrum investigation. The colloid absorption spectrum was recorded using a Hitachi U3410 spectrophotometer from Japan. In order to acquire micrographs of the resultant nanoparticles, a TEM (JEM-200 CX) at 200 kV has been employed. The PM 580 dye,
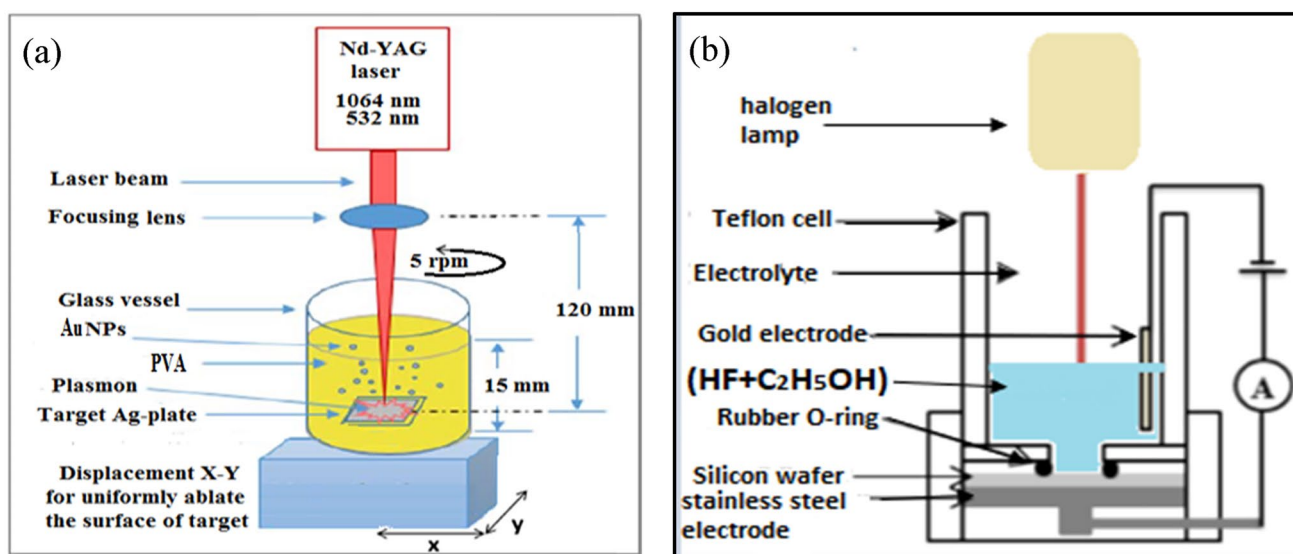

Fig. 1 The experimental set-up of the **a** colloidal Au/Ag NPs production and **b** photoelectrochemical etching technique

whose molecular formula is $C_{22}H_{33}BF_2N_2$ and molecular weight 374.32 g/mol, was obtained from Merck Sigma-Aldrich CO. Bearing a weight of 0.03743 g as a powder, it was dissolved with 10 ml ethanol to obtain a solution of the PM 580 dye with an initial concentration of 0.01 M. Then, this concentration was diluted to obtain concentrations that range from 10^{-6} to 10^{-9} M. Silicon wafers with orientation (100), n-type and thickness of 600 ± 25 µm were used. Porous Si is made using the photo-electrochemical etching (PECE) process. Halogen lamp as a source of light has been utilized with etching time (5, 10, 15, 20, and 25 min) and constant current density 30 mA/cm² as shown in Fig. 1b. The morphological and structural properties of the PSi layer and the SERS-effectual substrate were studied using the FE-SEM techniques. Raman spectra of these samples were examined using a Sunshine Raman spectrometer system and after they were excited by a laser source with a wavelength of 532 nm, where the objective

lens (50×). The laser power was 4.2 mW, and the integration time was 2 s.

Results and discussion

The intensity of the PL increases with the increase in the time of etching, and peak shifting to high energy or lower wavelength as shown in Fig. 2a. The PL mechanism surface state presumes that the carriers' absorption happens in Si crystallites via the effects of the quantum confinement. The centers of the recombination are created by the atoms of Si at crystallite surface that adjusts the lengths of their bond as well as their angles for the purpose of accommodating the changes in the local conditions and energy gap increases in the porous Si results from confinement of the porous Si practical in lower dimension. As a result, the likelihood of recombination of the electrons and the holes represents low dimensional structure
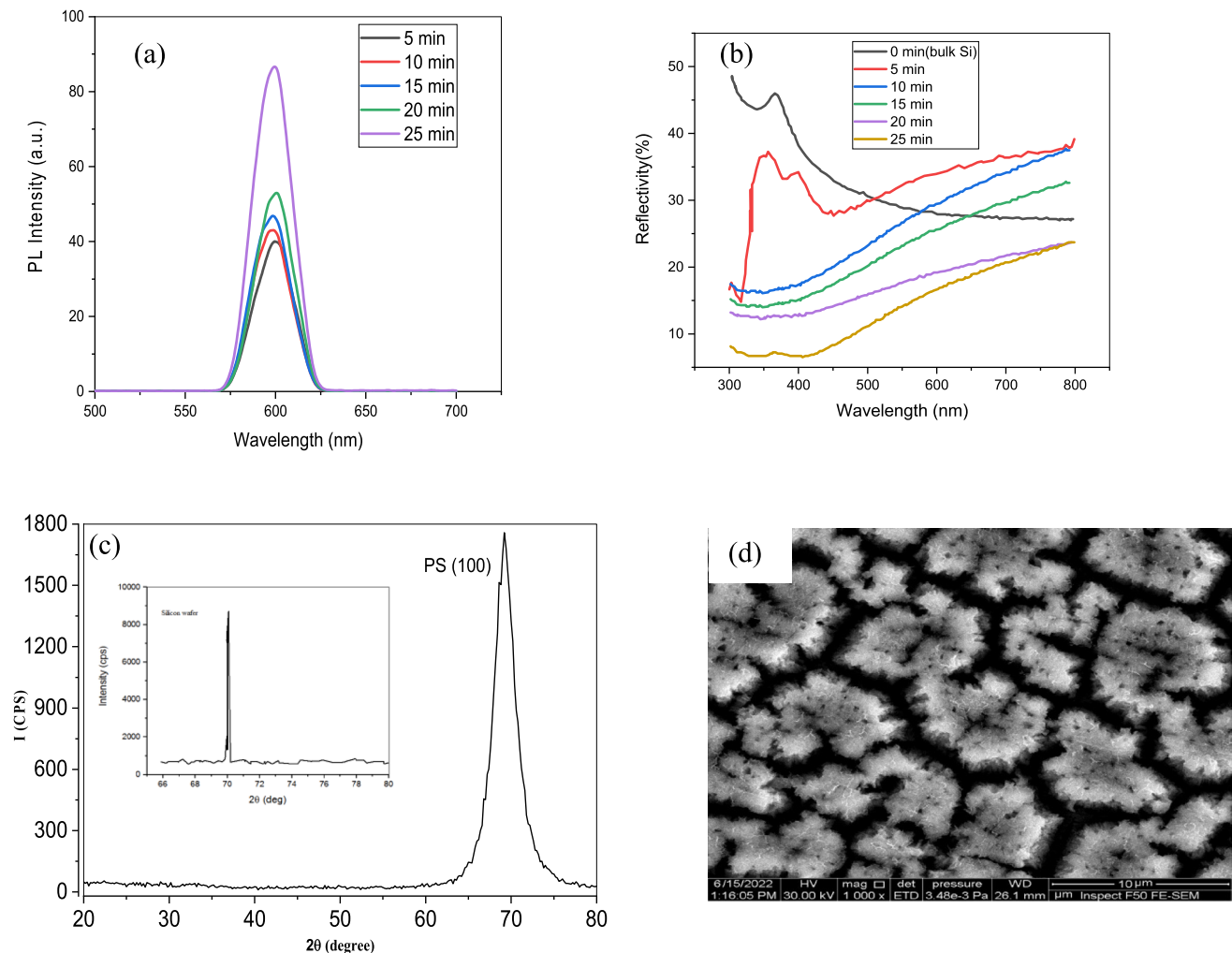

Fig. 2 **a** PL spectra of Porous Si at a variety of the etching time durations, **b** Reflectivity spectra of c-Si and Porous Si samples with various etching times, **c** the patterns of the XRD of c-Si (left) and Porous Si, **d** SEM of Porous Si that had been prepared with 25 min etching time

and such agreement with practical in box theory as demonstrated in Table 1. Band-energy gap (E_g) is increased with the increase in the time of etching with the use of Eq. 1 [33] and the decrease in the wave-length as a result the effect of the quantum confinement leads to the decrease in the value of the refractive index (n) Eq. 2 [34]. Evidently, the value of PL spectra excitation of 602 nm can be visible, with blue shifting in band-gap in comparison with the bulk Silicon, and that is a result of quantum confinement effect (QCE). Figure 2b illustrates porous Si reflection spectra in comparison with c-Si sample. R% Measurement of the Porous Si layers had shown that there is a potential of considerably reducing the reflectivity of the surface on the crystalline Silicon wafers through the formation of thin layer of the Porous Silicon through the anodization etching. Those results have shown that porous surface layer on the crystalline Si in fact enhances efficiency through acting like ARC layer. Silicon bulk has high level of the reflectance in the case where PS layer roughness is improved. Which might be associated with development of several of pore layers, and that has been considered to improve the diameter of the pore. In addition to that, the larger the diameter of the pores, the higher was their effectiveness, which is shown in Fig. 2b. The Porous Silicon crystallite size has been researched with the use of the XRD analysis, and crystalline degree of the etched sample has been calculated with the use of the XRD as shown in Fig. 2c. The results of the Bulk Si XRD exhibit a highly sharp peak, $2\theta = 69.92°$, and show wafer's single crystalline structure with the altering full-width at half maximum (FWHM) for a 25 min etching duration and 30 mA/cm^2 current density, this peak becomes highly broad. The PS structure SEM images which have been obtained for 25 min etching duration are shown in Fig. 2d; it has been noticed when the time of the etching has been increased, average diameter of the pore is changed. The Porous Si has sponge-like structure with extensively branching pore, which can be observed from image.

$$E = \frac{hc}{\lambda} \tag{1}$$

$$n = \sqrt{1 + \frac{A}{B + E_g}} \tag{2}$$

where $A = 13.6$ eV, $B = 3.4$ eV, h: Plank constant, c: speed of light.

Figure 3a presents the spectra of absorption for the Au/Ag NPs colloidal suspensions that have been synthesized by 532 nm wave-length of the laser irradiation with the use of various laser pulse energy values. Figure 3b shows the dependence of fundamental characteristics of absorption Plasmon band (APB), which is its center wave-length, FWHM, and maximal intensity on laser pulse energy. Based on results, the center wave-length as well as FWHM do not show any considerable dependences upon laser pulse energy, those results suggested that the size as well as the size distribution of nano-particles are similar in studied interval of pulse energy. Nonetheless, intensity of APB is increased over 40% in a case of the increase in laser pulse energy (LPE) from 200 to 1000 mJ, which suggests the increase of [Au/AgNPs] as laser energy has been increased. For the purpose of studying the impact of laser wave-length 532 nm, the samples have been made through the variation of laser pulse energy from 400 to 1000 mJ. The time of the ablation has been kept constant for all of the samples at 5 min (1000 laser pulses). Figure 3c and d shows TEM image and Au:Ag core:shell NPs size distribution. The Au NPs have been found spherical in their shape with the size in a range between 25 and 35 nm. In the case where the silver target has been ablated in gold colloidal suspension, Au:Ag core:shell NPs formation and growth happens. It is interesting to note that particles in proximity of the plasma plume expansion geometry become large particles in comparison with other particles and after that, as soon as the size is increased, in turn causing more gold ions to become attached to particle as a result of an increase in the surface area.

Figure 4a illustrates the spectra of absorbance of Au/Ag NPs suspensions that have been prepared for different laser pulse energy, the utilized wave-length used has been $\lambda = 1064$ nm. Figure 4b illustrates the dependence of the parameters of surface plasmon resonance (SPR) as laser pulse energy function. The spectra of the absorption show an absorption band about 400–550 nm, which is one of the Ag NP feature. One band of absorption has been observed at 400 and 600 mJ laser energy. This could be one of the consequences of low amounts of the formed Au/Ag NPs. TEM image of similar sample that has been utilized for Fig. 4 has been reported in Fig. 4c. Au/Ag NPs synthesized by laser pulses at 1064 nm (1000 mJ), show clear crystalline structure, and they have small sizes and prevalently spherical shapes.

From what we see in the distribution of Au nanoparticles on the surface of the membrane, there is a discrepancy in
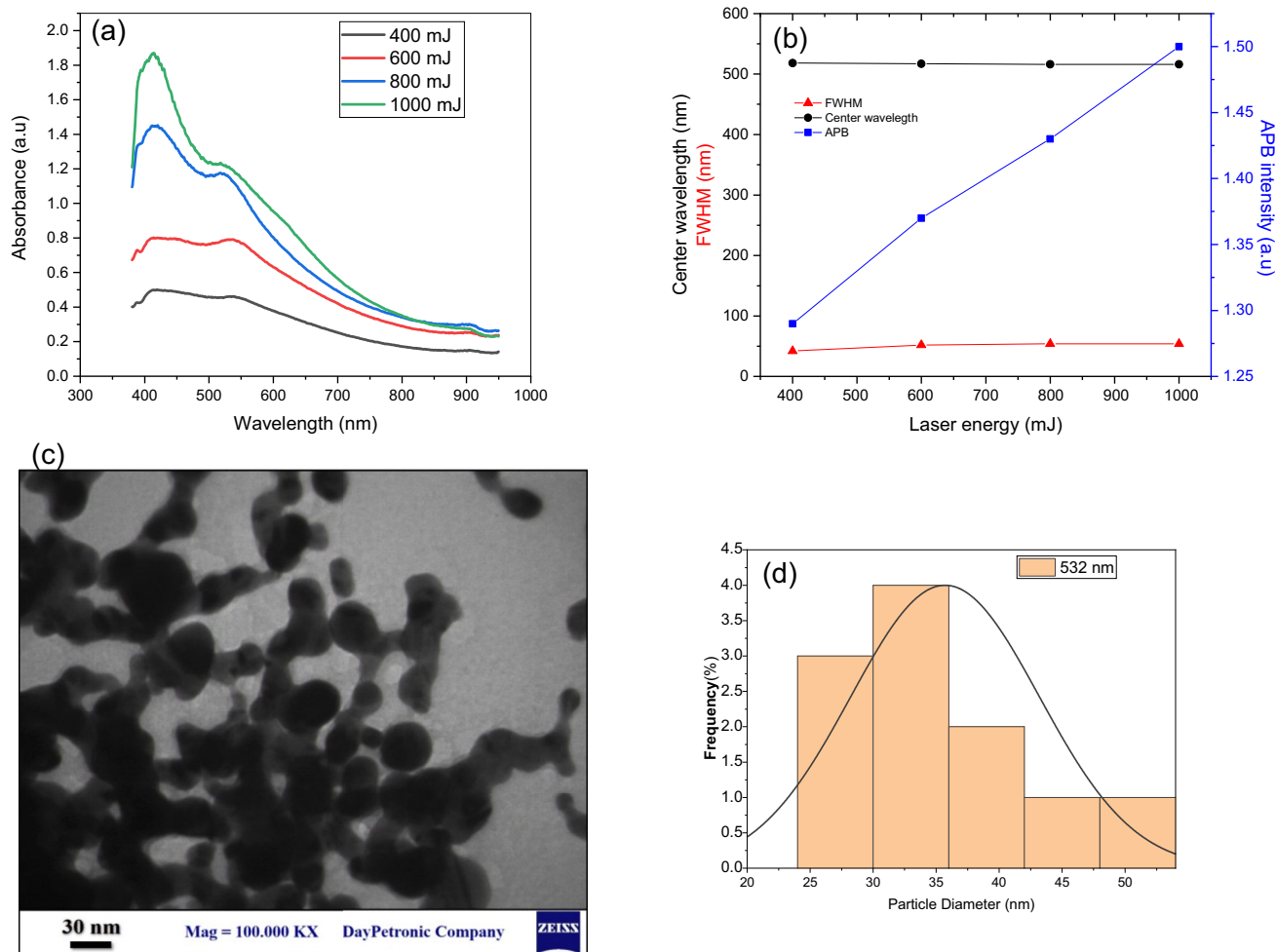
Table 1 Values that have been obtained from the PL peaks Porous Silicon with various etching times

Etching time	λ (nm)	E_g (eV)	n
5 min	602	2.0598	1.8684
10 min	601	2.0632	1.8679
15 min	600.5	2.0649	1.8677
20 min	600	2.0666	1.8675
25 min	599	2.0701	1.8671

Fig. 3 **a** Absorption spectra of Au/AgNPs that have been synthesized by $\lambda = 532$ nm, and LPE between 400 and 1000 mJ. **b** FWHM, center wave-length, and APB versus LPE. **c** TEM image of Au/AgNPs **d** and their Au/Ag NP size distribution that had been produced in PVA produced via laser ablation ($\lambda = 532$ nm, $f = 1$ Hz, $E_p = 1000$ mJ/pulse)

the distribution process. In addition, the homogeneity was in varying proportions and different from 532 to 1064 nm. Furthermore, regarding the Ag nanoparticles, it was noticed an increase in aggregation, where this increase in the laser energy (532 nm) leads to the increase in the aggregation, where the greater the laser energy used in preparing the nanomaterial, the greater the concentration of this substance and sometimes an increase in granular size as a result of the assembly process occurring in nanomaterials, as is clear to us through Figs. 3 and 4.

The nature of crystal growth and the phases in which the prepared Au/Ag thin film on PS substrate with two laser wavelength (532 nm and 1064 nm) and laser pulse energy of 1000 mJ/pulse were determined using X-ray diffraction are shown in Fig. 5a and b, respectively. The diffraction planes of Au/Ag NPs with 1000 mJ/pulse at (111), (200), (220), and (311) belong to 2θ value equal to 37.833, 44.03, 64.37, and 77.49, respectively, which matched with JCPDS

CARD-No: (00-004-0784). Broad FWHM, small crystalline size, have been observed for Au/Ag NPs with optimal energy of 1000 mJ/pulse which attributed to the increasing of crystallinity and the surface become more homogenous by rearrangement of atoms within the structure. The behavior of X-ray diffraction pattern of Au/Ag NPs synthesized by1064 nm wavelength has the same diffraction peaks all other laser energies with increasing in intensity, especially for strong preferred orientation (111) at $2\theta = 37.833°$.

Results of these calculations are presented in Table 2. As the size of the crystallite has been estimated by Scherrer approach may be limited for Au/AgNPs, this result has been considered as adequate estimation for nano-crystal diameter. Estimated size of the crystallite is different for every one of the reflections, which suggests the fact that the NPs are not perfect spheres.

The ability of the prepared substrates Au:AgNPs-532 nm/PS and Au:AgNPs-1064 nm/PS to improve SERS signals
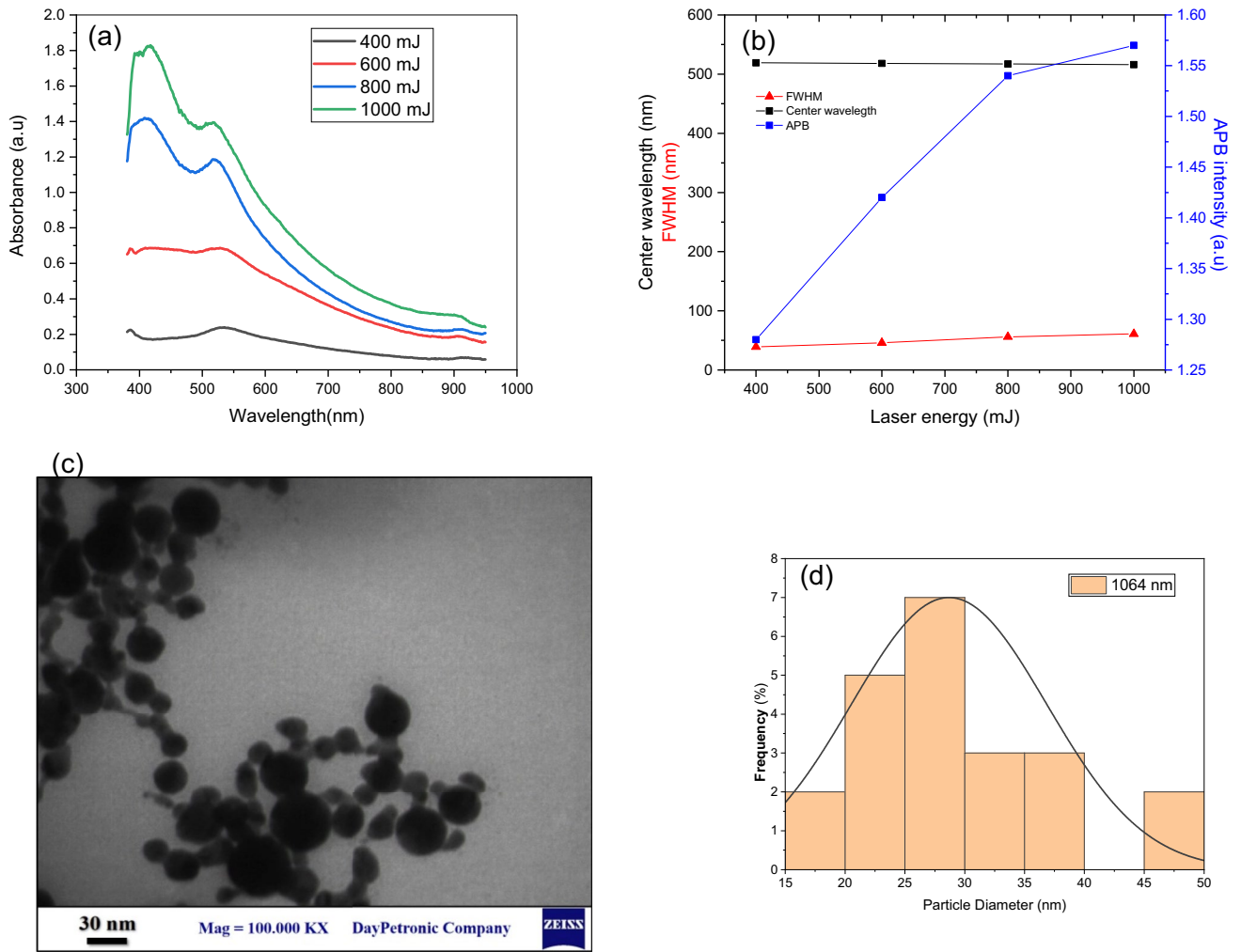
Fig. 4 **a** Absorption spectra of Au/AgNPs that have been synthesized by $\lambda = 1064$ nm, and LPE between 400 and 1000 mJ. **b** FWHM, center wave-length, and APB versus LPE. **c** TEM image of Au/AgNPs **d** and their size distribution of Au/AgNPs that had been produced in PVA produced via laser ablation ($\lambda = 1064$ nm, $f = 1$ Hz, $E_p = 1000$ mJ/pulse)
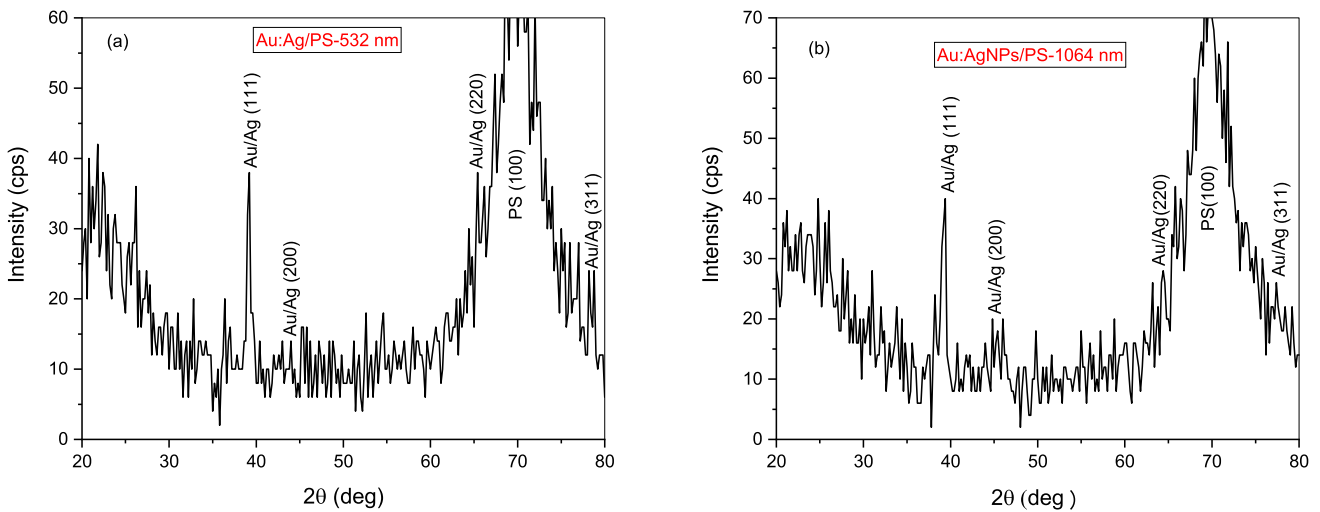

Fig. 5 Shows the XRD patterns for Au:AgNPs/PS prepared with the use of various laser wavelengths **a** 532 nm, **b** 1064 nm

Table 2 Crystallites size obtained by means of Scherrer equation of Au/Ag NPs which prepared under different laser wavelength at LPE 1000 mJ

Sample	hkl	2θ (°)	d_{hkl} (nm)	FWHM (°)	C.S (nm)
Au:Ag-532 nm	111	38.990	0.2414	0.3951	17.832
	200	44.870	0.2726	0.1815	38.150
	220	64.520	0.3857	0.0986	64.159
	311	78.760	0.5602	0.2421	23.968
Au:Ag-1064 nm	111	38.991	0.2414	0.5655	12.456
	200	44.634	0.2755	0.1499	47.020
	220	64.572	0.3871	0.4345	13.089
	311	78.423	0.4531	0.2638	22.081
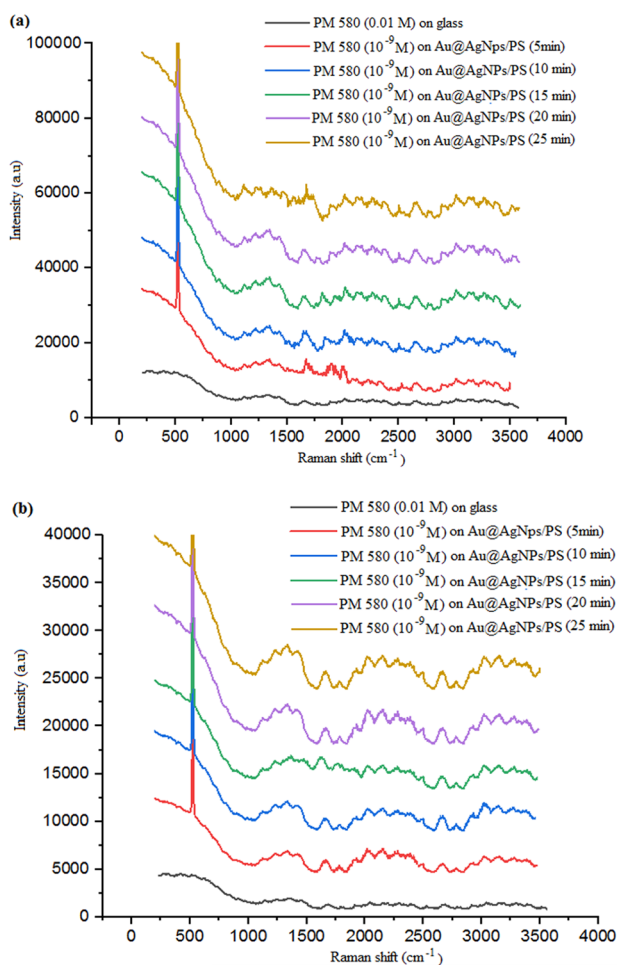
Fig. 6 Raman shifts of PM 580; SERS spectra with Au:AgNPs/PS as substrates obtained by **a** 532 laser ablation wavelength. **b** 1064 nm laser ablation wavelength

and test their ultra-sensitivity was demonstrated using the PM 580 dye as probe molecules as shown in Fig. 6a and b. The normal Raman spectrum of pure PM 580 molecule at a concentration of 0.01 M is coated on glass. It also illustrates

the PM 580 molecule spectra deposited on the Au:Ag/PS prepared by different etching time effectual substrates. Nanostructures were deposited and desiccated onto porous silicon and then onto the PM 580 dye in 10^{-9} M concentration. After being excited by a laser source with a 532 nm wavelength and 4.5 mW of power, all samples revealed SERS activity and distinctive peaks. The locations of wavenumber peaks (1116, 1215, 1334, and 1657 cm^{-1}) correspond to the modes, accordingly (C–H in-plane bend), (C–H in-plane bend), (N–H in-plane bend), and (C–C stretching) are assigned in Table 3. Raman shifts in spectral ranged from 400 to 35,000 cm^{-1} with a detection limit of 10^{-9} M. It was discovered that the peak intensity of Raman signals increased as etching time of PS increased, showcasing a linear correlation between the peak intensity of Raman signals and PS etching time. Furthermore, in Au:AgNPs/PS nanostructures, such nanogaps between adjacent Au:AgNPs and nano-spacer between PS helped achieve an excellent SERS signal. The wavenumber peak of 1657 cm^{-1} was used to compute the enhancement factors (EFs) of the SERS signal of PM 580 dye on the Au:AgNPs-532 nm/PS and Au:AgNPs-1064 nm/PS. substrates, and the following equation was utilized to compute the SERS EFs [35].

$$EF = \frac{I_{SERS}}{I_{RS}} \frac{C_{RS}}{C_{SERs}} \tag{3}$$

where I_{RS} & I_{SERS} represent intensity of normal Raman without nanostructures and SERS spectrum of probe molecules. C_{RS} and C_{SERS} represent analyte probe concentrations in bulk of PM 580 (0.01 M) and SERS of PM 580 (10^{-9} M) sample, respectively. As a result, the SERS EFs of PM 580 (10^{-9} M) reached (13.7×10^7) and (5.6×10^7) at the wavenumber peak 1657 cm^{-1} for the effectual substrates Au:AgNPs-532 nm/PS and Au:AgNPs-1064 nm/PS, respectively. The coupling between LSP of Au@AgNPs and the many texturing PS of the Si nanostructures created via the Au/Ag decoration on the surfaces of the Au:AgNPs/PS nanostructures produced a strong stimulation of the SERS signal by improving the EM field at texturing.

Conclusion

Laser ablation of the pure gold and silver sheets in PVA might be used to generate Au:AgNPs. Ultra-fine Au:AgNPs have been generated through using a shorter laser wavelength. While basic laser wave-length (longer wavelength) may be utilized to manufacture smaller sizes with greater concentrations, low laser energy also results in smaller elliptical-shaped sizes. In this work, laser pulse energies of 0.4–1 J/pulse have been utilized in ablation process; the absorption spectra of particles have been found as highly

Table 3 Raman bands of the normal as well as the SERS spectra of PM 580 molecule that had been obtained with Au:AgNPs/PS substrates synthesized at 532 nm laser wavelength

Normal Raman (cm^{-1})	SERS (cm^{-1}) etching time of PS					Assignment
	5 min	10 min	15 min	20 min	25 min	
1112	1114	1113	1112	1115	1116	C–H in-plane bend
1210	1212	1213	1213	1214	1215	C–H in-plane bend
1316	1332	1334	1334	1332	1333	N–H in-plane bend
1653	1655	1656	1655	1656	1657	C–C stretching

sensitive to ablation energy. According to TEM images, an increase in the ablation energy causes core–shell particles to grow and create. These colloidal Au:Ag core–shell deposited on Si nanostructures were shown to have potential SERS activity. PM 580 was used as probe molecule, as well as Raman enhancement is in a range of 10^7. SERS spectra have been found as spectral dependent and improvement of different Raman bands in the case where etching time for PS and laser wavelength is changed, maintaining all other experimental conditions constant. It is feasible to develop a wide range of effective substrates and obtain sensitive, reliable detection in biological and chemical fields by employing this manufacturing process.

Author contribution QKH: Conceptualization, preparation samples, Writing- Original draft. ANA: Preparation, Visualization, Investigation, Supervision, analysis, Validation. FA-HM: Methodology, Writing—Reviewing and Editing.

Declarations

Conflict of interest Authors would like to declare that they do not have any conflict of interests.

References

1. M. Aswad, F.A.-H. Mutlak, M. Jabir, S. Abdulridha, A. Ahmed, U. Nayef, Laser assisted hydrothermal synthesis of magnetic ferrite nanoparticles for biomedical applications. J. Phys. Conf. Ser. **1795**, 012030 (2021)
2. M. Abed, F.A.-H. Mutlak, A. Ahmed, U. Nayef, S. Abdulridha, M. Jabir, Synthesis of Ag/Au (core/shell) nanoparticles by laser ablation in liquid and study of their toxicity on blood human components. J. Phys. Conf. Ser. **1795**, 012013 (2021)
3. R. Mohammed, F. Mutlak, G. Saleh, Structural and optical properties of green spinach extract leaf (*Spincia olercea*) prepared with silver nanoparticles as antibacterial by effect of pulsed laser. J. Opt. **51**, 491–499 (2021)
4. M. Aswad, F.A.-H. Mutlak, Synthesis and structural characteristics of $Co_{1-x}Cu_xFe_2O_4$ magnetic ferrite nanoparticles using hydrothermal technique. Iraqi J. Phys. **17**, 10–20 (2019)
5. A. Ahmed, M. Abdulameer, M. Kadhim, F. Mutlak, Plasma parameters of Au nano-particles ablated on porous silicon produced via Nd-YAG laser at 355 nm for sensing NH_3 gas. Optik **249**, 168260 (2022)
6. N. Abdulkhaleq, U. Nayef, A. Albarazanchi, MgO nanoparticles synthesis via laser ablation stationed on porous silicon for photoconversion application. Optik **212**, 164793 (2020)
7. U. Nayef, R. Kamel, Bi_2O_3 nanoparticles ablated on porous silicon for sensing NO_2 gas. Optik **208**, 164146 (2020)
8. N. Abdulkhaleq, A. Hasan, U. Nayef, Enhancement of photodetectors devices for silicon nanostructure from study effect of etching time by photoelectrochemical etching technique. Optik **206**, 164325 (2020)
9. D. Jwied, U. Nayef, F.A.-H. Mutlak, Preparation and characterization of C: Se nano-rods ablated on porous silicon. Optik **239**, 166811 (2021)
10. N. Harb, F. Mutlak, Production and characterization of Tungsten Trioxide nanoparticles on porous silicon as photoconductive detector via pulsed laser deposition. Optik **257**, 168815 (2022)
11. F. Mutlak, A. Ahmed, U. Nyef, Q. Al-zaidi, S. Abdulridha, Improvement of absorption light of laser texturing on Silicon surface for optoelectronic application. Optik **237**, 166755 (2021). https://doi.org/10.1016/j.ijleo.2021.166755
12. E. Fazio, B. Gökce, A. De Giacomo, M. Meneghetti, G. Compagnini, M. Tommasini, F. Waag, A. Lucotti, C.G. Zanchi, P.M. Ossi, Nanoparticles engineering by pulsed laser ablation in liquids: concepts and applications. Nanomaterials **10**, 2317 (2020)
13. M. Rafique, M.S. Rafique, U. Kalsoom, A. Afzal, S.H. Butt, A. Usman, Laser ablation synthesis of silver nanoparticles in water and dependence on laser nature. Opt. Quantum Electron **51**, 179 (2019)
14. N.G. Semaltianos, Nanoparticles by laser ablation. Crit. Rev. Solid State Mater. Sci. **35**, 105 (2010)
15. D.S. Zhang, B. Göekce, S. Barcikowski, Laser synthesis and processing of colloids: fundamentals and applications. Chem. Rev. **117**, 3990 (2017)
16. R.M. Altuwirqi, A.S. Albakri, H. Al-Jawhari, E.A. Ganash, Green synthesis of copper oxide nanoparticles by pulsed laser ablation in spinach leaves extract. Optik **219**, 165280 (2020)
17. T. Rashid, U. Nayef, M. Jabir, F.A.-H. Mutlak, Study of optical and morphological properties for Au–ZnO nanocomposite prepared by laser ablation in liquid. J. Phys. Conf. Ser. **1795**, 012041 (2021)
18. F.A.-H. Mutlak, R. Jamal, A. Ahmed, Pulsed laser deposition of TiO_2 nanostructures for verify the linear and non-linear optical characteristics. Iraqi J. Sci. **62**(2), 517–525 (2021)
19. T. Rashid, U. Nayef, M. Jabir, F.A.-H. Mutlak, Synthesis and characterization of Au:ZnO (core:shell) nanoparticles via laser ablation. Optik **244**, 167569 (2021)

20. D. Jwied, U. Nayef, F.A.-H. Mutlak, Synthesis of C: Se nanoparticles ablated on porous silicon for sensing NO_2 and NH_3 gases. Optik **241**, 167013 (2021)

21. D. Jwied, U. Nayef, F. Mutlak, Improvement of responsivity of C: Se nanoparticles ablated on porous silicon. Optik **241**, 167222 (2021)

22. S. Khudiar, U. Nayef, F. Mutlak, Preparation and characterization of ZnO nanoparticles via laser ablation for sensing NO_2 gas. Optik **246**, 167762 (2021). https://doi.org/10.1016/j.ijleo.2021.167762

23. S. Khudiar, U. Nayef, F.A.-H. Mutlak, S. Abdulridha, Characterization of NO_2 gas sensing for ZnO nanostructure grown hydrothermally on porous silicon. Optik **249**, 168300 (2022)

24. S. Khudiar, F. Mutlak, U. Nayef, Synthesis of ZnO nanostructures by hydrothermal method deposited on porous silicon for photoconversion application. Optik **247**, 167903 (2021)

25. J.W. Jeon, S. Yoon, H.W. Choi, J. Kim, D. Farson, S.H. Cho, The effect of laser pulse widths on laser—Ag nanoparticle interaction: femto-to nanosecond lasers. Appl. Sci. **8**(1), 112 (2018)

26. M. Garcia, Surface plasmons in metallic nanoparticles: fundamentals and applications. J. Phys. D Appl. Phys. **45**(38), 38950 (2018)

27. E. Giorgetti, A. Giusti, F. Giammanco, P. Marsili, S. Laza, Dendrimer-capped nanoparticles prepared by picosecond laser ablation in liquid environment. Molecules **14**(9), 3731 (2009)

28. A. Hamad, L. Li, Z. Liu, A comparison of the characteristics of nanosecond, picosecond and femtosecond lasers generated Ag, TiO_2 and Au nanoparticles in deionised water. Appl. Phys. A **120**(4), 1247 (2015)

29. E.B. Kaganovich, I.M. Krischenko, S.A. Kravchenko, E.G. Manoilov, B.O. Golichenko, A.F. Kolomys, V.V. Strel'chuk, SERS spectroscopy of nanocomposite porous films containing silver nanoparticles. Opt. Spectrosc. (2015). https://doi.org/10.1134/s0030400x1502007

30. R. Pilot, R. Signorini, C. Durante, L. Orian, M. Bhamidipati, L. Fabris, A review on surface-enhanced Raman scattering. Biosensors **9**, 57 (2019). https://doi.org/10.3390/bios9020057

31. E.C. Le Ru, P.G. Etchegoin, Sub-wavelength localization of hot-spots in SERS. Chem. Phys. Lett. (2004). https://doi.org/10.1016/j.cplett.2004.08.065

32. A.M. Alwan, L.A. Wali, A.A. Yousif, Optimization of AgNPs/mesoPS active substrates for ultra-low molecule detection process. Silicon (2018). https://doi.org/10.1007/s12633-018-9758-7

33. A. Alber, F. Mutlak, The role of various etching time in Si nanostructures for ultra-high sensitivity photodetector. Optik **265**, 169427 (2022)

34. E.M. Sulaiman, U.M. Nayef, F.A.-H. Mutlak, Structural, morphological, photoluminescence, and sensitivity of Au:TiO_2 nanoparticles via laser ablation on porous silicon. J Opt (2022). https://doi.org/10.1007/s12596-022-00930-z

35. M. Chaja, T. Kramer, B. Neuenschwander, Influence of laser spot size and shape on ablation efficiency using ultrashort pulse laser system. Procedia CIRP **74**, 300 (2018)